Journal of the Serbian Society for Computational Mechanics / Vol. 17 / No. 2, 2023 / pp 1-15
(10.24874/jsscm.2023.17.02.01)

A MULTISCALE MULTIPHYSICS FINITE ELEMENT FOR LUNG

Miloš Kojić[1,2,3]

[1] Houston Methodist Research Institute, Department of Nanomedicine, 6670 Bertner Ave., Houston, TX 77030
[2] Bioengineering Research and Development Center BioIRC Kragujevac, 6 Prvoslava Stojanovića Street, 3400 Kragujevac, Serbia
[3] Serbian Academy of Sciences and Arts, 35 Knez Mihailova Street, 11000 Belgrade, Serbia

Abstract

The previously formulated finite element for lung mechanics (MSCL) by the author is extended to include airflow and molecular transport by diffusion. The lung mechanics is analyzed in detail providing an insight into the deformation of the microstructural elements. Also, some refinements are introduced with respect to the previous model. Here, the finite element is extended to incorporate airflow and convective-diffusive particulate (molecular) transport. The smeared concept (the Kojic Transport Model – KTM) is implemented with lung small airway generations considered as subdomains within the KTM. The subdomains refer to a selected number of generations according to the airway diameters. Each domain has its own volumetric fraction and transport tensor specified in terms of the airway size. The computational procedure implemented in the PAK-BIO software consists of three passes within each time step: mechanics, airflow, and diffusion. The current geometry is used for the airflow where the alveolar sacs are considered as the source terms for the last domain, according to the rate of volumetric deformation and volumetric fraction of the sacs. The pressure distribution calculated in the pass 2 is used for the convective term in the diffusion. Here, the alveolar sacs are included as the last subdomain. The new element is now termed the General Lung Finite Element (GLFE). Coupling airflow in large airways, governed by the Navier-Stokes equations, to small airways (with the Hagen-Poiseuille equations) is presented; the same coupling is given for diffusion. Numerical examples illustrate the generality of the formulated finite element.

Keywords: Mechanics of lung microstructure, finite element, airflow and diffusion, Kojic Transport Model, multi-scale multiphysics 3D model, General Lung Finite Element (GLFE), lung tissue material models, surfactant.

1. Introduction - a review of constitutive relations for the cardiac tissue

We first give basic information regarding lung morphology. An overview of the lung airway structure can be seen in Fig. 1. The air flows into the lung starting from the trachea which branches into two bronchi and further continues to smaller bronchi and bronchioles. As shown in the figure, small airways (going from 5mm to 0,5mm in diameter) forming the bronchial tree, are classified into airway generations (divided into 23 generations). The smallest, the terminal bronchioles, are connected to the lung microstructure with the alveolar system composed of the alveolar ducts and sacs. Altogether, the airway system is a length of around 2,400 kilometers, with 300 to 500 million alveoli where the gas (nitrogen and oxygen) exchange occurs.

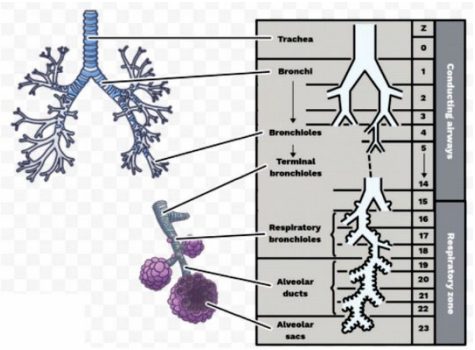

Fig.1. Lung morphology. The airway system starts from the trachea and ends in the lung microstructure with alveolar ducts and sacs.

For the completeness of this paper, we present an overview of generally accepted physiological models of lung mechanics, as in our paper (Kojic, 2020). These models were the most relevant for our initial finite element formulation of a 3D multiscale composite finite element (MSCL). Also, we give the basic physiological data important for modeling airflow and particulate transport within the lung airway system.

The generally accepted formulation of the mechanical lung model is given in the seminal publications of Weibel (1963) and Weibel and Gil (1977) where they introduced a fundamental concept of the loading-carrying system of the lung. The basic microstructural unit is represented by a duct, shown in Fig. 2a. Further, the model has been specified in Wilson and Bachofen (1982) in a way shown in Fig. 2b. Therefore, according to these models, there exists a system of two groups of fibers – here called external and internal fibers, which are carrying the mechanical forces within the lung; these fibers are called (Weibel, 2013) peripheral and axial fibers. Note that alveoli, shown in the figure, are connected to these two systems of fibers, therefore they serve as the connective tissue carrying the load, which will be used as the basis for our finite element model.

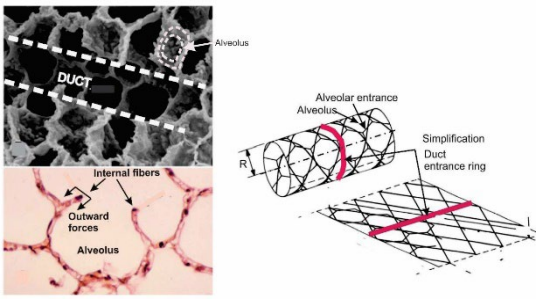

Fig.2. Microstructural model of Weibel. a) Scanning electron micrographs of a rabbit lung - duct and alveoli with forces acting on the internal fibers. b) Fibers and alveoli in the duct, (according to Wilson and Bachofen,1982), and the duct entrance ring as simplification used in our model.

Regarding the internal system of fibers, it is important to emphasize that, according to the mentioned references and Greaves et al. (2010), there is a balance of forces as schematically

shown in Fig. 3. It can be seen that the force produced by the internal ring is in balance with alveolar tissue and surfactant forces which, on the other hand, load the external fiber system. It follows that the internal (ring) fibers serve to keep the alveoli open, so that the entire microstructure behaves as a 'tensegrity' structure (Fuller, 1961; Ingber, 2003). Further, surfactant, covering the microstructural tissue, also plays an extremely important role in lung functioning. Namely, the surfactant has a hysteretic character (shown here in the description of material models) when the surface expands and then returns back, producing hysteretic deformation of the alveolar surfaces. This hysteresis further causes vorticity in the air within alveoli that facilitates gas exchange, of vital importance for life. We will include the surfactant mechanical action in our models.

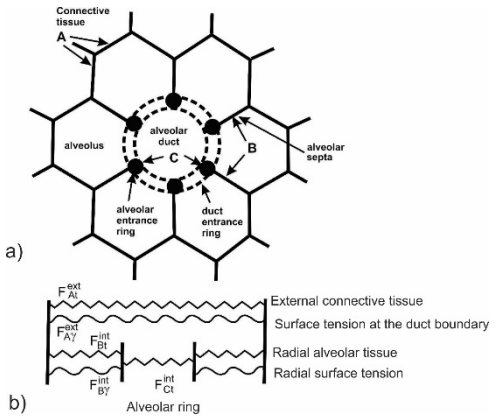

Fig.3. Alveolar duct model according to Greaves et al. (2010). a) Schematic of the duct structure which includes external tissue (A) connected to alveoli, with alveolar septa (B) and entrance rings, and duct entrance ring (C); b) Forces generated by microstructural deformation: F_{At}^{ext} and $F_{A\gamma}^{ext}$ - external connective tissue and surfactant, F_{Bt}^{int} and $F_{B\gamma}^{int}$ - radial alveolar tissue and surfactant, and F_{Ct}^{int} alveolar and entrance ring.

2. Our multiscale-multiphysics finite element for mechanics, airflow, and particulate (molecular) transport

Here, we extend the formulation of our FE element for mechanics (Kojic, 2020) to include airflow and particulate (molecular) transport. First, we review, with some refinements, the microstructural mechanics formulated in Kojic (2020).

The following approach is adopted in the application of the microstructural model. Considering the lung parenchyma as a 3D continuum, we have that the state of deformation at a material point is quantified by the stretches $\lambda_x, \lambda_y, \lambda_z$ in the global coordinate system x,y,z. Assuming isotropy, we use a mean stretch as a measure for the microstructural deformation, i.e.

$$\lambda = \left(\lambda_x + \lambda_y + \lambda_z\right)/3 = 1 + \left(e_{xx} + e_{yy} + e_{zz}\right)/3 = 1 + e_V \tag{1}$$

where e_{xx},e_{yy},e_{zz} are strains and e_V is the volumetric strain. We note that stretches can be determined from the deformation gradient (Kojic and Bathe, 2005). This stretch in our model represents the radial stretch of the duct external fibers so that, using geometry in Fig. 4b, we have the following relations:

$$R + R_a = \lambda\left(R_0 + R_{a0}\right) \tag{2}$$

$$R / R_0 = \lambda_R, \quad \lambda_a = R_a / R_{a0} \tag{3}$$

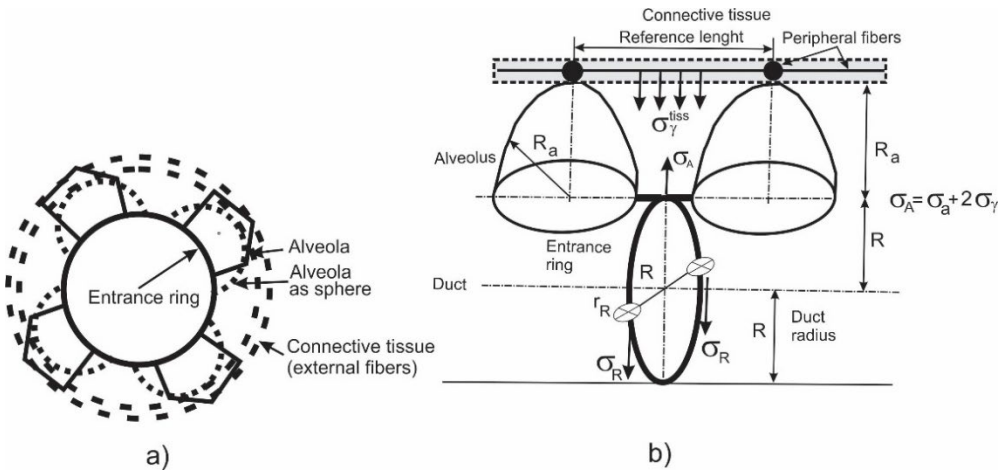

Fig.4. Microsrtuctural model (Kojic, 2020). a) Axial view of the duct with the entrance ring and alveoli approximated by semispheres; b) Entrance ring of the radius R and cross-sectional radius r_R, and alveoli (semi-spheres of radius R_a) covered by surfactant. The duct is connected to peripheral (external) radial and axial fibers of the connective tissue. The stresses loading the microstructural elements are displayed.

where R_0 and R_{a0} are values for the undeformed state. The fundamental balance equation between the external loading transferred between alveoli and ring can be written as

$$2\sigma_R r_R^2 \pi = \frac{1}{2} 2R_a \pi n_R \left(\sigma_a + 2\sigma_{a\gamma}\right)\delta_a \tag{4}$$

where n_R is the number of alveoli per ring, r_R is the radius of the ring cross-section, σ_R is stress within the ring, δ_a is alveolar thickness, σ_a is the stresses in the alveolar tissue due to deformation; and $\delta_{a\gamma} = \gamma / \delta_a$ is stress due to surfactant on both sides of the alveolus, with γ being the surface tension. Note that we have neglected radial rings of the model in Fig. 3, as in Kojic et al (2011). The alveolar ring is composed of smooth muscle cells and connective tissue cells, with the volumetric fraction m (Kojic et. al. 2011), so that (4) can be modified to

$$2r_R^2\left[m\sigma_{mus} + \left(1-m\right)\sigma_{ct}\right] = R_a \delta_a n_R \left(\sigma_a + 2\sigma_{a\gamma}\right) \tag{5}$$

where σ_{mus} and σ_{ct} are stresses within muscle and connective tissue fractions, respectively. The stress σ_γ^{tiss} acting on the external connective tissue can be expressed by the following relation

$$\sigma_\gamma^{tiss} = n_R \frac{\left(\sigma_a + 2\sigma_{a\gamma}\right)\delta_a}{2\left(R + R_a\right)} \tag{6}$$

Assuming that the external duct surface is also covered by the surfactant, there is additional stress loading the external tissue. This stress can be determined from the virtual work of surfactant on the external surface, ending by the expression

$$\sigma_{atissue}^{\gamma} = 2\frac{r_{Va}}{1-r_{Va}}\frac{\gamma}{\left(R+R_a\right)} \tag{7}$$

where r_{Va} is the air volumetric fraction.

We next formulate a multiscale-multiphysics finite element for the lung, termed a General Lung Finite Element (GLFE) which represents an extension of the previous finite element for lung mechanics (MSCL) in (Kojic, 2020). This new finite element is shown in Fig. 5.

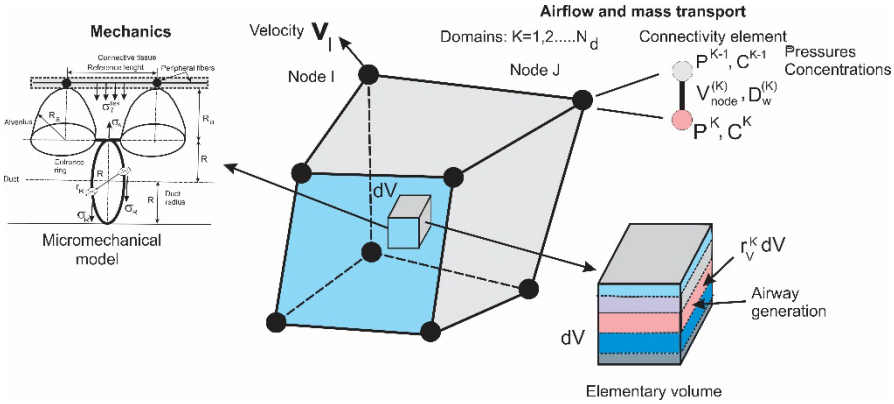

Fig.5. General finite element for lung (GLFE) as a multiscale-multiphysic finite element which includes mechanics, airflow, and mass transport.

We further give details on mechanics, followed by airflow, and mass transport.

2.1 Mechanics.

The balance equation for a finite element has a standard form (Kojic et al. 2022)

$$\left(\frac{1}{\Delta t}\mathbf{M}+\mathbf{K}\right)^{(i-1)}\Delta\mathbf{V}^{(i)} = \mathbf{F}^{ext(i-1)} + \mathbf{F}_V^{(i-1)} - \mathbf{F}^{\text{int}(i-1)} + \frac{1}{\Delta t}\mathbf{M}^{(i-1)}\mathbf{V}^t \tag{8}$$

for a time step Δt and equilibrium iteration i, where $\mathbf{V}$ are nodal velocities, $\mathbf{M}$ and $\mathbf{K}$ are mass and stiffness matrices; $\mathbf{F}^{\text{ext}}$, $\mathbf{F}_V$, and $\mathbf{F}^{\text{int}}$ are external, volumetric, and internal forces; and $\mathbf{V}^t$ is the velocity at the start of a time step. This balance equation can also be written in terms of displacements. The expressions for the matrices and nodal vectors are given elsewhere (e.g. Kojic et al. 2022). The specificity here is that the integration volume corresponds to the volumetric fraction of the external connective tissue, for example:

$$\mathbf{F}^{\text{int}(i-1)} = \int_V r_V^{tiss}\mathbf{B}_L^{T(i-1)}\boldsymbol{\sigma}^{(i-1)}dV \tag{9}$$

where r_V^{tiss} is the tissue volumetric fraction which can be expressed in terms of the air volumetric fraction as $r_V^{tiss} = 1\text{-}r_{Va}$, $\mathbf{B}_L$ is the strain-displacement matrix, and $\boldsymbol{\sigma}$ is the stress tensor within the connective tissue. Using the above analysis of microstructural deformation, the stress in (9) is

$$\sigma_{ii} = \sigma_{ii}^{tiss} + \sigma_{\gamma}^{tiss} + \sigma_{atissue}^{\gamma}, \quad ii = 1,2,3, \ no\ sum\ on\ i \tag{10}$$

where σ_{ii}^{tiss} is stress due to the deformation of external connective tissue.

Further are presented some details regarding the evaluation of stresses. We use the constitutive relationships shown in Fig. 6. From the current stretch calculated from displacements and strains according to (1), we determine the stresses σ_{ii}^{tiss} according to the uniaxial curve in Fig. 6a.

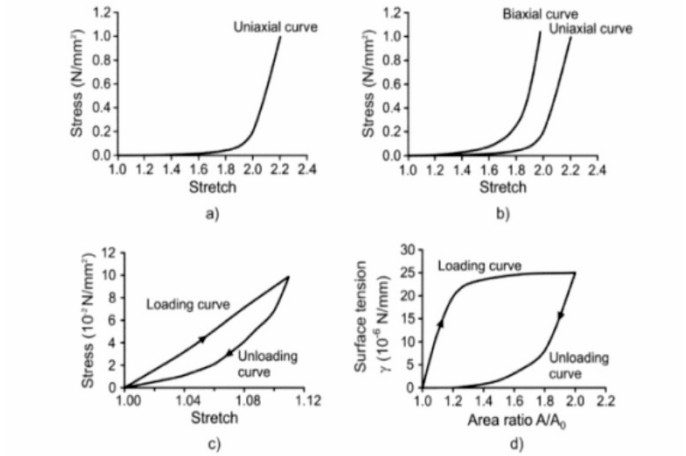

Fig.6. Constitutive curves for lung. a) Uniaxial model for entrance ring connective tissue and external connective tissue; b) Biaxial model for alveolar tissue; c) Hysteretic model for muscle tissue of the entrance ring; d) Hysteretic characteristic of surfactant.

In order to find other stress terms within the microstructure, it is necessary to determine deformations of the alveoli and entrance ring. Here, we solve the balance equation (5) as follows. The radius R of the ring is taken as a parameter such that equation (5) is satisfied. From geometrical relations, it can be found that the minimum and maximum values of R are:

$$R_{\min} = R_o, \quad R_{\max} = \lambda R_0 \tag{11}$$

Then, using a simple bisection procedure for the range R_{min} -R_{max}, we calculate:

- Current R
- Stretch $\lambda_R = R/R_0$, stress in the ring using λ_R and constitutive curves in Fig. 6a,c
- Stretch of alveolus λ_a from $R_a = \lambda\,(R_0+R_{a0})-R$, $\lambda_a = R_a/R_{a0}$ and stress σ_a form constitutive curves in Fig. 6b, using the biaxial curve
- Alveolar area ratio $\lambda_{a\gamma} = R_a^2 / R_{a0}^2$ and surface tension γ using constitutive curve in Fig. 6d, and then stress $\sigma_{a\gamma} = \gamma / \delta_a$
- External surface area ratio $\lambda_{ext\gamma} = \left(R + R_a\right)^2 / \left(R_0 + R_{a0}\right)^2$, surface tension using the constitutive curve in Fig. 6d, and external stress $\sigma_{atissue}^{\gamma}$ from (7)

During the solution process over time steps, we also update the air volumetric fraction as $r_{Va} = \eta r_{Va0}$, where:

$$\eta = \frac{\pi\left(R+R_a\right)^2 L_{duct}}{\pi\left(R_0+R_{a0}\right)^2 L_{duct0}} = \lambda\frac{\left(R+R_a\right)^2}{\left(R_0+R_{a0}\right)^2} = \lambda^3 \tag{12}$$

Here, L_{duct} and L_{duct0}, are current and initial duct lengths, and with the isotropy assumption $L_{duct} / L_{duct0} = \lambda$.

2.2 Airflow.

The airflow in large vessels can be modeled using 3D or axisymmetric 2D Navier-Stokes equations, or by approximate 1D Hagen-Poiseuille flow. The finite element balance equations for the Navier-Stokes model including incompressibility condition, and using the mixed formulation, can be written as (e.g. Kojic et al. 2022):

$$\begin{bmatrix} \frac{1}{\Delta t}\mathbf{M}+\tilde{\mathbf{K}}_{vv}^{(i-1)} & \mathbf{K}_{vp} \\ \mathbf{K}_{vp}^T & \mathbf{0} \end{bmatrix} \begin{Bmatrix} \Delta\mathbf{V}^{(i)} \\ \Delta\mathbf{P}^{(i)} \end{Bmatrix} = \begin{Bmatrix} \mathbf{F}_{ext}^{(i-1)} \\ \mathbf{0} \end{Bmatrix} - \begin{bmatrix} \frac{1}{\Delta t}\mathbf{M}+\mathbf{K}_{vv}^{(i-1)} & \mathbf{K}_{vp} \\ \mathbf{K}_{vp}^T & \mathbf{0} \end{bmatrix} \begin{Bmatrix} \mathbf{V}^{(i-1)} \\ \mathbf{P}^{(i-1)} \end{Bmatrix} + \begin{Bmatrix} \frac{1}{\Delta t}\mathbf{M}\mathbf{V}^t \\ \mathbf{0} \end{Bmatrix} \tag{13}$$

with the matrices given in this reference. The solution is obtained for velocity **V** and pressure **P**. In the case of the Hagen-Poiseuille flow model, we have the fluid pressure as a variable and the FE balance equations are

$$\mathbf{K}_p^{(i-1)}\Delta\mathbf{P}^{(i)} = \mathbf{Q}_p^{ext(i-1)} - \mathbf{K}_p^{(i-1)}\mathbf{P}^{(i-1)} \tag{14}$$

where $\boldsymbol{Q}_p^{ext}$ is external nodal fluid flux (which cancels at the internal FE nodes). The 2x2 transport matrix is

$$K_{p11} = K_{p22} = -K_{p12} = -K_{p21} = \frac{\pi d^4}{128\mu} \tag{15}$$

where d is the airway diameter and μ is air viscosity.

The small airways within the lung parenchyma are modeled by a continuum according to the Kojic Transport Model (KTM) (Kojic et al. 2022). We introduce flow domains by grouping airway generations into a specified number of domains, according to the airway diameter size. The 3D continuum balance equations have the form (14), but for 3D conditions, with the equivalent Darcy transport tensor

$$k_{Dij} = \frac{\pi}{128\mu A_{tot}}\sum_J d_J^4 \ell_{Ji}\ell_{Jj} \tag{16}$$

where d_J are airway diameters, and l_{Ji} are directional cosines of J small airways in the vicinity of the considered point within the parenchyma. Connectivity elements are assigned to nodes of 1D (pipe) elements when the pipe elements have permeable walls or when they branch into smaller airways used in the smeared fields. Also, it is assumed that all subdomains of the KTM are interconnected. The 2-node transport matrix for these elements has the form (15), i.e. for a node J we have

$$K_{J11} = K_{J22} = -K_{J12} = -K_{J21} = h_{pJ}V_J \tag{17}$$

where h_{pJ} is the permeability (resistance) coefficient, and V_J is the volume of the continuum belonging to the node. We use the permeability coefficient to be proportional to the mean value of diagonal terms of transport tensor and inversely proportional to the airway diameter at the

node. The alveolar sacs are included in the model as source terms within the last domain of the KTM, computed as

$$q_V = r_{Vsac} dV / dt \tag{18}$$

where r_{Vsac} is the sac volumetric fraction, while dV/dt represents the rate of the volume change evaluated in the mechanical model (pass 1 in the computational procedure described below).

2.3 Mass Transport (Diffusion).

Particulate (molecular) transport within the air is modeled as a diffusion with convection. The mass balance equation for a finite element and a domain K can be written as (Kojic et al., 2022)

$$\left(\frac{1}{\Delta t}\mathbf{M}+\mathbf{K}+\mathbf{K}^v\right)^{K(i-1)}\Delta\mathbf{C}^{K(i)} = \mathbf{Q}^{KS(i-1)}+\mathbf{Q}^{KV(i)}-\left(\frac{1}{\Delta t}\mathbf{M}+\mathbf{K}+\mathbf{K}^v\right)^{K(i-1)}\mathbf{C}^{K(i-1)}+\frac{1}{\Delta t}\mathbf{M}^K\mathbf{C}^{Kt} \tag{19}$$

where **C** are nodal concentrations, while expressions for the matrices are given the reference. The same form of the balance equation applies to large airways where the airflow is governed by the Navier-Stokes equations. We here include the alveolar sacs as a domain with its diffusive characteristics. The air velocities entering into the convection matrix $\mathbf{K}^v$ are used from solutions of the airflow. The diffusion tensor for the parenchyma subdomains is computed from the expression analogous to (16), i.e.

$$D_{ij} = \frac{1}{A_{tot}}\sum_J A_J D_J \ell_{Ji}\ell_{Jj} \tag{20}$$

where A_J and D_J are cross-section areas and diffusion coefficients, respectively. The connectivity elements are defined as in the case of airflow, with diffusion coefficients to be used in (17) instead of the hydraulic resistance coefficients h_{pJ}.

3. Connection between continuum (2D or 3D) and 1D FE models

In practical applications, there can be a need to connect continuum (2D or 3D) models and more efficient 1D models. A schematic of the connection is shown in Fig. 7. Regarding the fluid (air)

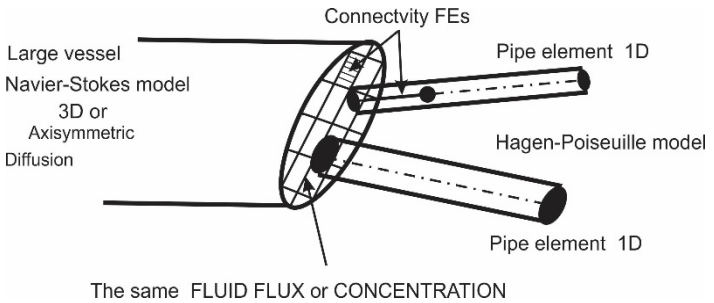

Fig.7. Schematics of connection of large vessel and smaller pipe elements.

flow we use the Navier-Stokes equations (13) for a large vessel and pipe elements with equation (14) for pipe elements. Equation (13) is based on the force balance at the nodes, while equation (14) relies on the mass flux balance at the pipe nodes. Therefore, since there is no compatibility

of the nodal quantities, it is not possible to have a direct coupling, with the common nodes at the boundary. Then, we compute nodal fluxes at large vessel nodes as

$$\mathbf{Q}_{bound\ node} = \sum_{bound\ el} \left[\frac{1}{\Delta t}\mathbf{M} + \mathbf{K}_{vv}^{(i-1)} \quad \mathbf{K}_{vp} \right] \begin{Bmatrix} \mathbf{V}^{(i-1)} \\ \mathbf{P}^{(i-1)} \end{Bmatrix} + \frac{1}{\Delta t}\mathbf{M}\mathbf{V}^{t} \tag{21}$$

A convergence criterion is checked for the system of equations (13). Further, the sum of nodal fluid fluxes (21) is used in the balance equation (14) as $\mathbf{Q}_p^{ext(i-1)}$, and the system of equations for the pipe structure is solved for pressures. The convergence is checked and the procedure of successive solutions continues until convergence criteria are satisfied for both domains.

In the case of diffusion, a common mesh which includes large vessels and pipes is generated and the solution is obtained in a standard incremental procedure, with the corresponding boundary conditions. Convective terms are computed from velocities of air available from the solution of the airflow. It is imposed, as a logical approximation, that all nodes at the common boundary in both domains have the same concentration.

4. Finite element model for the entire lung

In this section, a concept of the entire lung model is summarized using the above description of finite elements for mechanics, airflow, and diffusion. The lung model is shown in Fig. 8. It can be seen that large airways have the same equation numbers for velocities with the surrounding continuum. In the case of airflow and diffusion, large airways are not connected to the surrounding continuum, while smaller airways modeled by 1D pipe elements may have a connection (connectivity elements) with the first domain of the composite smeared 3D finite elements (GLFEs).

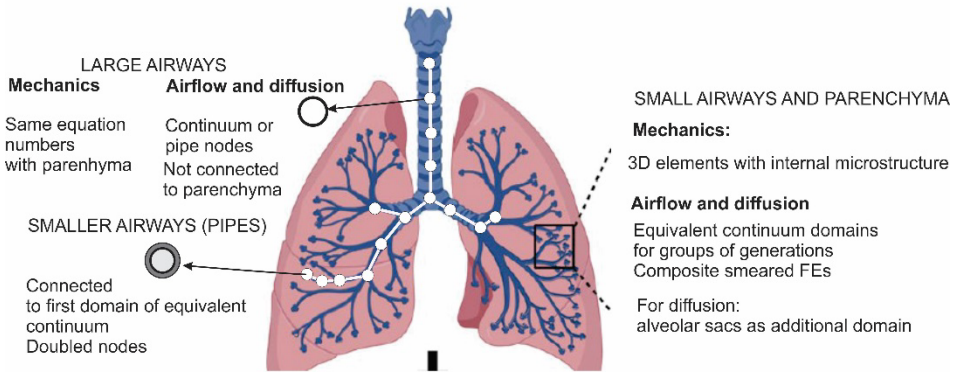

Fig.8. Finite element model for the entire lung. The model includes mechanics, airflow and diffusion. Connectivities between domains are shown in the model.

These finite elements and computational procedure according to details given in Fig.8 are built in our finite element code PAK-BIO (Kojic et al. 2018). The following computational steps (passes) are implemented into the code for each time step:

- Pass 1 – **Mechanics**. Velocities and displacements of the solid are determined.

- Pass 2 – **Airflow**. Geometry and velocity field of the solid are used from Pass 1. Airflow is determined by computing the pressure field. In the case of coupling 2D or 3D models with the pipe 1D elements, two separate FE meshes are generated and two systems of equations are successively solved within iterations until convergence is reached for both systems.
- Pass 3 –**Diffusion**. Geometry and velocity field of the air are used from passes 1 and 2. In the case of coupling a 2D or 3D model with the pipe elements, one finite element mesh is generated and one system of equations is solved until convergence criteria are satisfied.

5. Numerical examples

Here, we selected two examples to demonstrate the main characteristics of the developed lung model.

5.1 Example 1 – Three-axial stretch

One element is subjected to high stretches in all directions, as shown in Fig. 9. The stretch increases up to the value of displacements 1 [mm] and then decreases to zero, simulating a lung cycle, as shown in the figure; hence doubling the element size. We impose these high stretching to emphasize the character of the deformation of microstructural elements. The goal of the example is to gain insight into these deformations which are of vital importance for lung function (Kojic et al. 2011). Regarding the microstructural data, we have used (lengths in [mm]):

- entrance ring radius R= 0.1, entrance ring cross-section radius r_R =0.05, alveolus radius R_a= 0.2, alveolus thickness δ_a= 0.01; ratio muscle/connective tissue in entrance ring m=0.2; radial alveolar density n_R=6.

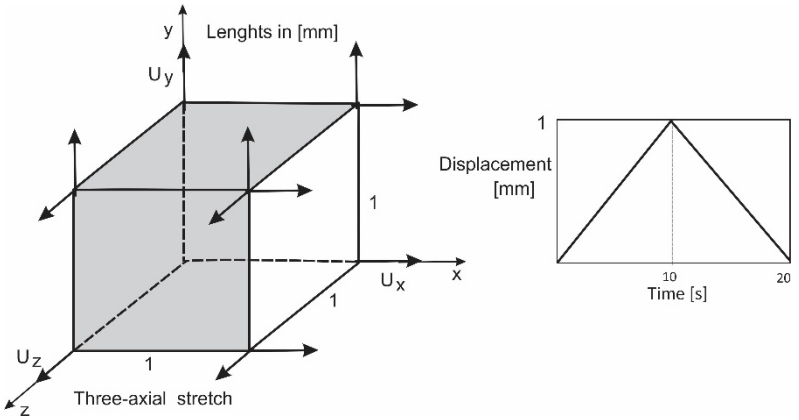

Fig.9. Three-axial stretch of the General Lung Finite Element (GLFE).

Figure. 10 shows a change of the duct volume (relative to the initial) and internal ring size over a cycle. It can be seen that the volume changes nonlinearly without hysteresis since the change of the external boundary does not have hysteretic character (Fig. 9). On the other hand, due to the hysteresis of surfactant and internal ring (Figs. 6c,d) the internal ring radius displays hysteresis – with the size larger in the unloading (lung expiration), Fig.10b.

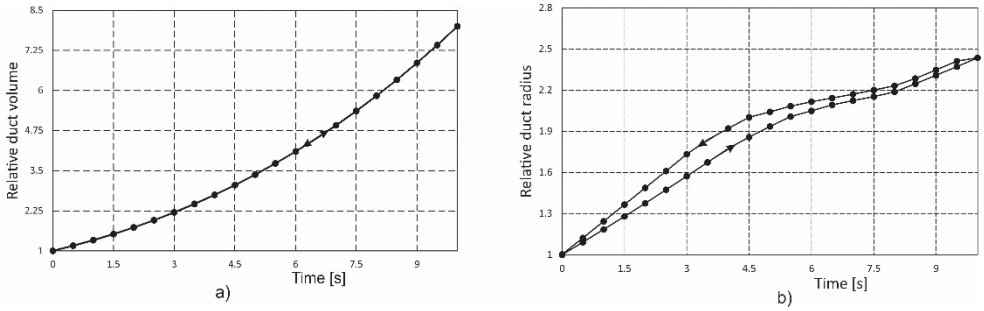

Fig.10. Change of the duct volume a), and internal ring size b), over a lung cycle (time during unloading-expiation goes from 10 to 0).

Further, in Fig 11a is shown the dependence of the duct relative radius on the relative duct volume, with hysteretic character as in Fig, 10b. Fig 11b shows a hysteretic relationship of the relative duct (alveolar) surface on the relative duct volume, which is termed geometric hysteresis in Kojic et al (2011). The hystereses shown in Figs. 10b and 11 are of vital importance since they enhance nitrogen-oxygen gas exchange as the fundamental process in living organisms. Hysteresis produced by surfactant is so important that a baby born with surfactant deficiency needs immediate medical intervention.

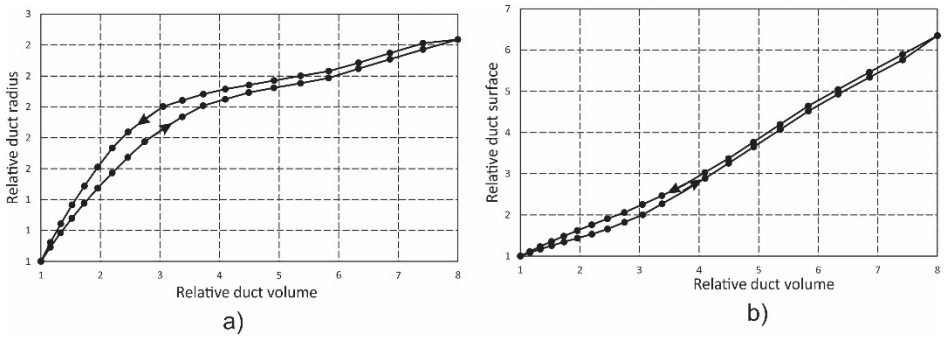

Fig.11. a) Relative entrance ring (duct) radius vs. relative duct volume; b) Relative duct surface in terms of the relative duct volume.

5.2 Example 2 – Coupling between large and small vessels

In a simple example shown in Fig. 12 we illustrate coupling between two domains according to the procedure introduced in this study. As shown in Fig. 12, we consider a fluid domain (3D or axisymmetric, boundary elements 1-5) – on the left, coupled to four 1D pipe elements with boundary nodes 3,4,19,22. The parenchyma is modeled by two 3D GLFEs. The length of each fluid element is 2 [mm] while the length of each of the GLFEs is equal to 1 [mm]. Axial symmetry is assumed for fluid, with an approximately parabolic profile at the entering left surface and velocity at the symmetry line equal to 1 [mm/s]. It is taken that fluid density is equal to 0.001 [g/mm^3] and viscosity 0.001 [Pas]. Constant concentration is prescribed at the left entrance equal to 1 [M]. It is assumed that the prescribed velocity increases linearly during the inspiration period of 10s and linearly decreases to zero at time 20s (time function shown in Fig. 9); the diffusion coefficient is D=10 [mm^{2}s^{-1}].

The fluid domain is connected to the parenchyma through four pipes with boundary nodes 3,4,19,22. The diameters of pipes are taken to be 2 [mm]. We have used a very small elasticity modulus for pipes (E=0.001Pa) to emphasize the mechanical response of the lung parenchyma. It can be seen that connectivity elements between pipes and GLFEs are 3-11, 4-9, 19-1,.., 24-14. The hydraulic proportionality coefficient is 0.7. Pressure and concentration at the pipe end nodes are imposed to be zero. It is adopted that there are 4 groups of small airways (generations) with diameters (in [mm]): 2, 1.5. 1, 0.5, and equal volumetric fractions r_V=0.1. The last domain represents the alveolar sacs. The solid is subjected to three-axial uniform mechanical loads, with fixed left and back surfaces with sliding conditions on these surfaces. Maximum force at nodes is $3x10^{-4}$ [N] for nodes at edges and $6x10^{-4}$ [N] for other nodes.

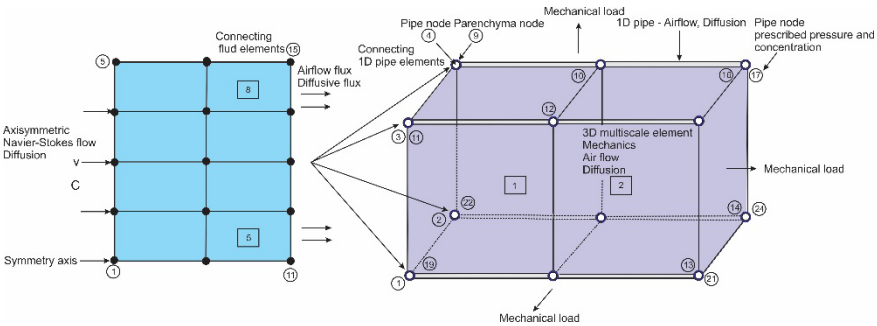

Fig.12. Two models coupled. 3D or axisymmetric fluid domain (left) coupled to 1D (pipe) model within a 3D parenchyma model (3D GLFE elements). Boundary fluid elements 5-8 are connected to boundary pipe nodes 3,4,19,22.

The goal of this example is to show a mechanical hysteretic character of the overall solid continuum and to illustrate airflow and diffusive mass transfer from the continuum fluid to pipe structure. Fig. 13 shows the normal displacement of the right surface over a cycle, with a hysteresis. In Fig. 14 pressures within pipe and subdomains are shown. Pressures increase linearly at inspiration and then decrease during expiration. There is no hysteresis in pressure. It can be seen that pressure decreases over domains, with the decrease becoming smaller from the first to the last domain.

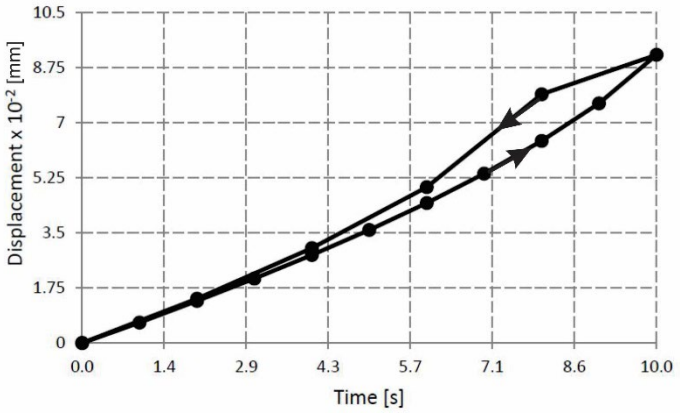

Fig.13. Displacement of the right solid surface over a cycle (time during unloading goes from 10 to 0).

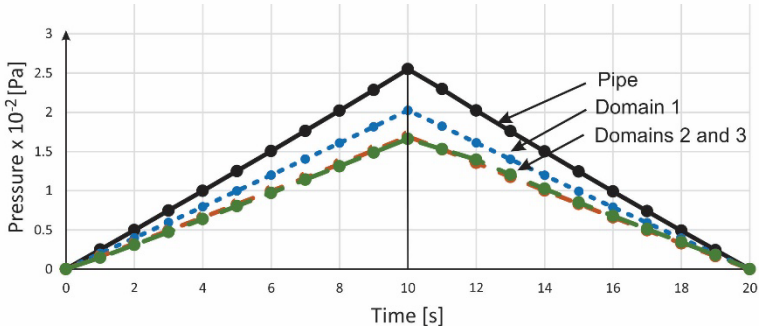

Fig.14. Pressure within pipe connections with fluid and for a point within small airway domains over time. There is no notable hysteresis over the cycle.

Figure 15 shows a change in concentration. To emphasize the differences between inspiration and expiration periods, we draw the graphs within the time=1-10 in inspiration, and time=10-0 at expiration. It can be seen from Fig. 15a that concentration at the connecting surface increases nonlinearly during inspiration and almost linearly decreases with a small slope.

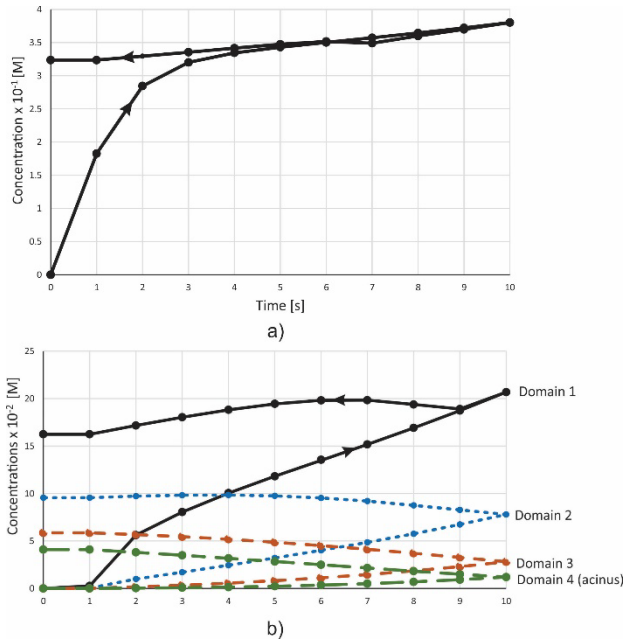

Fig.15. a) Concentration at the connection of pipes with fluid over time; b) Concentration over time at a point close to pipe connection with fluid, for the small airways domains.

Fig. 15 displays that, although concentration at the entrance of fluid is constant, there is a decrease at the entrance of pipes because the pressure gradient decreases affecting the convective part of diffusion. A similar change of concentration over time occurs in domain 1 of parenchyma

(Fig. 15b), while in other parenchyma domains, concentration change is almost symmetric in the two time periods since the convection effects are smaller. A jump in concentration at time 10 sec. within the first domain is due to a large change in the pressure gradient in pipes at that time

6. Summary and concluding remarks

We have developed a multiscale-multiphysics finite element for lung mechanics, airflow, and mass transport (General Lung Finite Element, GLFE). The element is multiscale in all these three fields since it includes microstructural deformation of the lung parenchyma and multiscale smeared methodology for gradient-driven physical fields (Kojic Transport Model). It offers the possibility of modeling the lung in a simple way because the lung parenchyma can be modeled by 3D continuum elements which are connected to large airways. It is also shown how the 1D pipe elements can be connected to 3D models for airflow and mass transport.

Simple examples illustrate the main features of the formulated element, with results showing an agreement with experimental observations reported in the enormous number of references. Further applications to the real conditions might lead to possible modifications of the current model. The author believes that applications to real lung geometry and physiological conditions will prove that the presented methodology can serve as a basis for the development of a software tool for research and clinical practice.

Acknowledgments: The author acknowledges continuous support from the City of Kragujevac, Serbia, National Cancer Institute under grant U01CA244107-01, and the Serbian Academy of Sciences and Arts, Grant F-134. The author is thankful to Dr. Akira Tsuda, and to Dr. James P. Butler, Harvard School of Public Health for earlier joint work in this field. Also, the author is thankful to his collaborators Prof. Miljan Milosevic, Dr. Vladimir Simic, and Dr. Bogdan Milicevic for the development of the CAD interface and further testing of the developed model.

References

Fukaya, H., Martin, C. J., Young, A. C., and Katsura, S. (1968). Mechanical Properties of Alveolar Walls, J. Appl. Physiol., 25(6), 689–695.

Fukuoka Y., Kawataa Y., Nikia N., Umetanib K., Nakanoc Y., Ohmatsud H., Moriyamae N., Itohf H. (2014). Microstructure analysis of the secondary pulmonary lobules by 3D synchrotron radiation CT, Medical Imaging: Computer-Aided Diagnosis, edited by Aylward S., Lubomir M. Hadjiiski, Proc. of SPIE Vol. 9035, 1-7.

Fuller B. (1961). Tensegrity. Portfolio and Art News Annual, 4, 112–127.

Greaves I. A., Hildebrandt J., Hoppin Jr. F. G. (2010). Micromechanics of the Lung, Handbook of Physiology – Chapter 14 The Respiratory System, American Physiological Society.

Henry F. S., Butler J. P, Tsuda A. (2002). Kinematically Irreversible Flow and Aerosol Transport in the Pulmonary Acinus: A Departure from Classical Dispersive Transport, J. Appl. Physiol., 92, 835–845.

Hildebrandt, J., Fukaya, H., and Martin, C. J. (1969). Stress-Strain Relations of Tissue Sheets Undergoing Uniform Two-Dimensional Stretch, J. Appl. Physiol., 27(5), 758–762.

Ingber D. E., Tensegrity I. (2003). Cell structure and hierarchical systems biology. J Cell Sci, 116,1157–1173.

Kojic M., Tsuda A. (2004). Gravitational deposition of aerosols from oscillatory laminar pipe flows, J. Aerosol Science, 35, 245-261.

Kojic M. and Bathe K. J. (2005). Inelastic Analysis of Solids and Stuctures, Springer.

Kojic M., Vlastelica I., Stojanovic B., Rankovic V., Tsuda A. (2006). Stress integration procedures for a biaxial isotropic material model of biological membranes and for hysteretic models of muscle fibers and surfactant, Int. J. Num. Meth. Engng., 68, 893-909.

Kojic M., Filipovic N., Stojanovic B., Kojic N. (2008). Computer Modeling in Bioengineering, J. Wiley and Sons.

Kojic M., Filipovic N., Milosevic M, (2018). PAK-BIO – Finite Element Program for Biomechanics and Coupled Problems, Bioeng. Research Center BIOIRC, Kragujevac, and University of Kragujevac, Serbia.

Kojic M., Butler J. P., Vlastelica I., Stojanovic B., Rankovic V., Tsuda A. (2011). Geometric hysteresis of alveolated ductal architecture, ASME J. Biomechanics, 133, 1- 11.

Kojic M., Milosevic M., Simic V., Ferrari M. (2014). A 1D pipe finite element with rigid and deformable walls, J. Serb. Soc. Comp. Mech., 8 (2), 38-53.

Kojic M. (2020). Multiscale composite 3d finite element for lung mechanics, J. Serbian Soc. Comp. Mech. 14(1), 1-11.

Kojic M, Milosevic M, Ziemys A (2022). Computational Models in Biomedical Engineering - Finite Element Models Based on Smeared Physical Fields: Theory, Solutions, and Software, Elsevier.

Liu C. H., Niranjan S. C., Clark J. W. Jr., San K. Y., Zwischenberger J. B., Bidani A. (1998). Airway mechanics, gas exchange, and blood flow in a nonlinear model of the normal human lung, J. Appl. Physiol. 84(4), 1447–1469.

Miki H., Butler J. P., Roger R. A., Lehr J. L. (1993). Geometric Hysteresis in Pulmonary Surface–to-Volume Ratio during Tidal Breathing, J. Appl. Physiol., 75(4), 1630–1636.

Sasaki, H., and Hoppin, F. G., Jr. (1979). Hysteresis of Contracted Airway Smooth Muscle, J. Appl. Physiol.: Respir. Environ. Exercise Physiol., 47(6),1251–1262.

Tsuda A., Henry F. S., Butler J. P. (1995). Chaotic Mixing of Alveolated Duct Flow in Rhythmically Expanding Pulmonary Acinus, J. Appl. Physiol., 79(3), 1055–1063.

Tsuda A., Filipovic N., Haberthu¨r D., Dickie R., Matsui Y., Stampanoni M., and Schittny J. C. (2008). Finite element 3D reconstruction of the pulmonary acinus imaged by synchrotron X-ray tomography, J Appl Physiol., 105, 964–976.

Tsuda A., Laine-Pearson F. E, Hydon P. E. (2011). Why Chaotic Mixing of Particles is Inevitable in the Deep Lung, J. Theor. Biol. 286, 57–66.

Weibel E. R. (2013). It Takes More than Cells to Make a Good Lung, Am J Respir Crit Care Med, 187(4), 342–346.

Weibel E. R. (1963). Morphometry of the human lung, Academic, New York. Journal of the Serbian Society for Computational Mechanics / Vol. 14 / No. 1, 2020.

Weibel E. R. and Gil J. (1977). Structure-function relationships at the alveolar level, Bioengineering Aspects of the Lung, New York, 3, 1-81.

Wilson, T. A. (1982). Surface Tension-Surface Area Curves Calculated from Pressure-Volume Loops, J. Appl. Physiol.: Respir. Environ. Exercise. Physiol., 53(6), 1512–1520.

Wilson T. A., and Bachofen H. (1982). A Model for Mechanical Structure of Alveolar Duct, J. Appl. Physiol., Respir. Environ. Excercise Physiol., 52(4), 1064–1070.